Supplemental Document

Biomedical Optics EXPRESS

Optical beam scanner with reconfigurable non-mechanical control of beam position, angle, and focus for low-cost whole-eye OCT imaging: supplement

MARÍA PILAR URIZAR,[1,2] ENRIQUE GAMBRA,[1] ALBERTO DE CASTRO,[2] ÁLVARO DE LA PEÑA,[2] ONUR CETINKAYA,[3] SUSANA MARCOS,[2,4] AND ANDREA CURATOLO[2,3,*]

[1] *2EyesVision S.L., Madrid, Spain*
[2] *Instituto de Óptica "Daza de Valdés", Consejo Superior de Investigaciones Científicas (IO, CSIC), Spain*
[3] *International Centre for Translational Eye Research (ICTER), Institute of Physical Chemistry, Polish Academy of Sciences (IPC-PAS), Warsaw, Poland*
[4] *The Institute of Optics and Flaum Eye Institute, Center for Visual Sciences, University of Rochester, New York, USA*
[*] *acuratolo@ichf.edu.pl*

Supplement DOI: https://doi.org/10.6084/m9.figshare.23618898

Parent Article DOI: https://doi.org/10.1364/BOE.493917

AN OPTICAL BEAM SCANNER WITH RECONFIGURABLE NON-MECHANICAL CONTROL OF BEAM POSITION, ANGLE AND FOCUS FOR LOW-COST WHOLE-EYE OCT IMAGING: SUPPLEMENTAL DOCUMENT

1. System parameters dependencies and limitations

An analysis of the optical beam scanner optomechanical parameters, such as the fixed mechanical distances between system components, was performed to optimize the design of optical beam scanner. This analysis was performed using Eqs. (1)-(9) with the goal of maximizing the scanning range of the optical beam scanner in both anterior and posterior segment scanning configurations, *i.e.*, Δh_{out} and $\Delta\theta_{out}$ for the telecentric and angular scans, respectively. During this analysis, two parameters of the beam scanner in the double pass setup were considered: the input offset h_{in} and the distance *d* between ETL_1 and ETL_2. The optical elements of the beam scanner are listed Table 1 of the main manuscript. The results of this analysis are shown in Fig. S1,S2. We always considered the start of either a telecentric or angular scan when the focal length of ETL_1 equaled that of ETL_2, *i.e.*, $f_1 = f_2$. This means that $h_{out} = -\, h_{in}$ in the starting position. The range h_{out} could vary in was between $|h_{in}|$ and the clear semi-aperture (CA) of ETL_2. CA is calculated as the semi-aperture minus the beam radius at ETL_2. This condition was imposed to avoid overlapping scan areas when considering the future implementation of the rotating HRM and periscope to perform radial, or concentric circular (or spiral) scans.

Fig. S1(a)-(c) show how the transverse scan range Δh_{out} varies as a function of the input offset h_{in}, while Figs. S1(d)-(f) show how the angular scan range $\Delta\theta_{out}$ varies as a function of the input offset h_{in}. The remaining distances are set as in Table 2 of the main manuscript, therefore the distance *d* between ETL_1 and ETL_2 was 150 mm, the distance between ETL_1 and the hollow roof mirror d_{HRM} was 30 mm, and the pivoting distance d_p from ETL_2 was 105 mm. In Figs. S1(a),(d) the transverse and angular scan ranges, respectively, are plotted as a function of the focal length f_1 of ETL_1 for different input offsets. The grayed-out area represents focal lengths that are too short and out of reach for ETL_1. In Figs. S1(c),(f) the transverse and angular scan ranges, respectively, are plotted as a function of the transversal displacement h_{out} of the beam from the axis of ETL_2 for different input offsets. The grayed-out area there represents displacements that are over the clear semi-aperture of ETL_2 and therefore out of bounds for ETL_2.

Figures S1(a),(d), show that the scan range increases with decreasing ETL_1 focal length and larger input offsets generate a larger scan range for a given focal length, while Figs. S1(c),(f) show that the scan range increases for larger transversal displacement h_{out} and smaller input offsets generate a larger scan range for a given transversal displacement. In Figs. S1(b),(e) the transverse and angular scan range, Δh_{out} and $\Delta\theta_{out}$, respectively, are plotted as a function of the input offset h_{in} considering these competing trends, up to the limits imposed by the shortest focal length f_1 of ETL_1 and the clear semi-aperture of ETL_2. For each input offset h_{in}, the smallest scan range determined by the most limiting factor is selected and plotted. The resulting curves have a peak at input offset $h_{in} = 2.5$ mm. This corresponds to half of the semi-aperture of ETL_1. Therefore, this value was selected as the optimal input offset, and resulted in Δh_{out} $= 2.5$ mm and $\Delta\theta_{out} = 1.2$ deg.

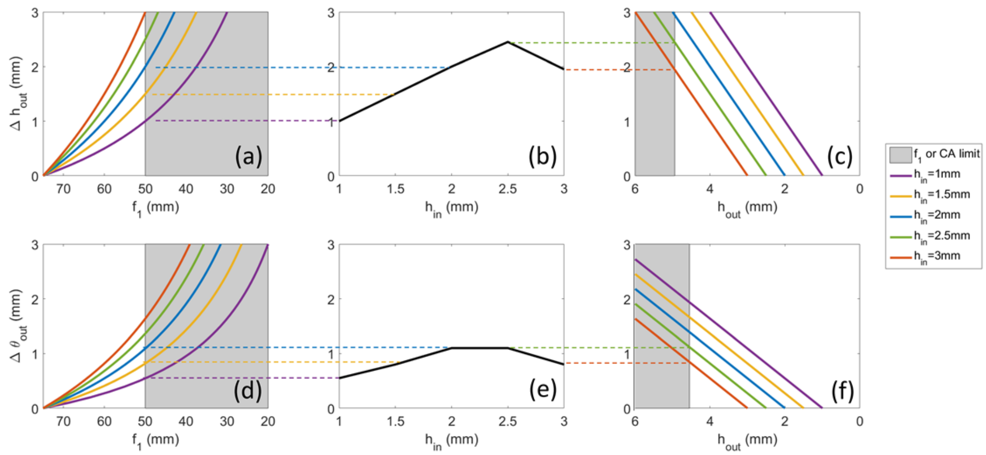

Fig. S1. Scan range variation as a function of the input offset h_{in} for the proposed beam scanner, where the components and other distances are listed in Tables 1,2. (a)-(c) The transverse scan range Δh_{out} variation as a function of the focal length f_1 of ETL_1, the input offset h_{in}, and the transversal displacement h_{out} of the beam from the axis of ETL_2, respectively. (d)-(f) The angular scan range $\Delta\theta_{out}$ variation as a function of same variables as in (a)-(c).

Similarly, Fig. S2 show how the transverse and angular scan ranges, Δh_{out} and $\Delta\theta_{out}$, respectively, vary as a function of the distance *d* between ETL_1 and ETL_2, when the input offset $h_{in} = 2.5$ mm, and all other distances are as those listed in Table 2 of the main manuscript. In Figs. S2(a),(d) the transverse and angular scan ranges, respectively, are plotted as a function of the focal length f_1 of ETL_1 for different values of the distance d. Again, the grayed-out area represents focal lengths that are too short and out of reach for ETL_1. In Figs. S2(c),(f) the transverse and angular scan range, respectively, are plotted as a function of the transversal displacement h_{out} of the beam from the axis of ETL_2 for different input offsets. As in Figs. S1(c),(f), the grayed-out area there represents displacements that are over the clear semi-aperture of ETL_2 and therefore out of bounds for ETL_2.

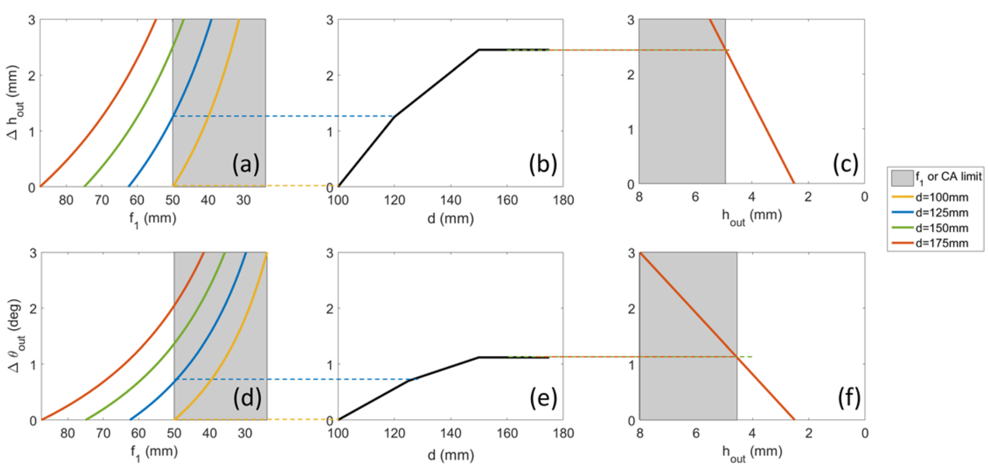

Fig. S2. Scan range variation as a function of the distance *d* between ETL_1 and ETL_2, for the proposed beam scanner, where the components and other distances are listed in Tables 1,2. (a)-(c) The transverse scan range Δh_{out} variation as a function of the focal length f_1 of ETL_1, the distance d, and the transversal displacement h_{out} of the beam from the axis of ETL_2, respectively. (d)-(f) The angular scan range $\Delta\theta_{out}$ variation as a function of same variables as in (a)-(c).

Figures S2(a),(d), show that the scan range increases with decreasing ETL_1 focal length and larger values of the distance between ETL_1 and ETL_2 generate a larger scan range for a given focal length, while Figs. S1(c),(f) show that the scan range increases with increasing transversal displacement h_{out} irrespective of the distance between ETL_1 and ETL_2. In Figs. S1(b),(e) the transverse and angular scan range, Δh_{out} and $\Delta\theta_{out}$, respectively, are plotted as a function of the distance d considering these competing trends, up to the limits imposed by the shortest focal length f_1 of ETL_1 and the clear semi-aperture of ETL_2. Again, for value of the distance d, the smallest scan range determined by the most limiting factor is selected and plotted. The resulting curves reach a plateau at $d = 150$ mm. Therefore, for device footprint considerations, this value was selected as the smallest distance that still resulted in $\Delta h_{out} = 2.5$ mm and $\Delta\theta_{out} = 1.2$ deg.

2. Experimental calibration of the ETL optical power

The control of the three ETLs was performed with a low-cost Arduino Nano board in combination with a custom Matlab GUI code that allowed to independently select the scan mode (telecentric or angular) and the working or pivoting distance of the output beam, d_f or d_p. The focal length or optical power of the ETLs was set by the duty cycle of a pulse width modulation (PWM) signal sent by the Arduino Nano board with 8-bit resolution to the lenses through a lens driver (DRV8833, Texas Instruments). Due to the high frequency of the PWM signal, the lenses are effectively subject to a voltage between 0-5 V proportional to the PWM signal. The focal length variation with voltage of each ETLs was characterized using a high speed focimeter and adjusted when aligned in the beam scanner experimental setup.

Figure S3 shows the experimental calibration for the look-up table between the 8-bit digital counts (0-255) of the PWM signal (at a given polarity) and the corresponding optical power (reciprocal of the focal length in meters) for ETL_1 in blue, ETL_2 in red, and of ETL_3 in yellow. The experimental data are shown as dots and they have been fitted to polynomial functions for later incorporation in the aforementioned Matlab GUI.

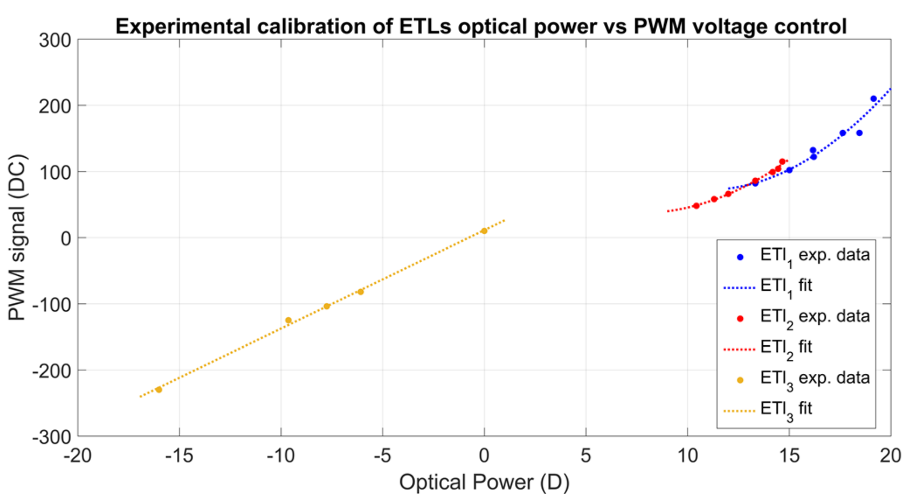

Fig. S3. Experimental calibration for the look-up table between the 8-bit digital counts (DC: 0-255) of the PWM signal and the corresponding optical power in diopters (D) for ETL_1 in blue, ETL_2 in red, and of ETL_3 in yellow.

Visualization 5 shows the changing PWM signal for ETL1 over time on an oscilloscope, while the beam profiler shows the focal spot size advancing laterally during repeated anterior scans, at a slower frequency for the sake of demonstration.